

# Multivalent Polyanionic 2D Nanosheets Functionalized Nanofibrous Stem Cell-based Neural Scaffolds

Yi Xia, Hua Yang, Shuang Li, Suqiong Zhou, Liyun Wang, Yuanjiao Tang, Chong Cheng,\* and Rainer Haag\*

Because developed neural cells are no longer regenerative and proliferative, achieving neural regenerations by using induced pluripotent stem cells (IPS cells) for nerve diseases have recently attracted much attention. Since the IPS cells' growth and differentiation can be manipulated by different physical and chemicals cues, scaffolds combining the beneficial nanostructures and extracellular matrix may become an ideal interface to promote IPS cells' neural differentiation. In this work, a biocompatible and multivalent polyanion, hyperbranched polyglycerol sulfate, is used to modify the graphene oxide to obtain bio-adhesive 2D nanosheets. After coating electrospinning nanofibers, the 2D nanosheets-functionalized nanofibrous scaffolds are applied to mediate the proliferation, lineage specification, and neural differentiation of IPS cells. The results suggest that the modified scaffolds can improve the adhesion and proliferation of IPS cells combined with high efficiency in maintaining their stemness. During the neural differentiation process, the scaffolds can promote neural differentiation and their maturity, meanwhile decreasing the lineage specification toward astrocyte. Overall, this study not only provides new multivalent/bio-adhesive nanofibrous scaffolds that integrate the chemical and physical cues to facilitate the targeted neural differentiation of IPS cells but also presents a novel pathway for the fabrication of carbon nanomaterials-based biocomposites in regenerative therapies.

(IPS cells) are frequently used while obviating the necessity to obtain the tissue from the human brain or take the ethical issues destroying embryos.<sup>[6–8]</sup> Moreover, the IPS cells are so sensitive that the cell behavior and cell differentiation fate could easily be affected by the dynamic microenvironment of the extracellular matrix (ECM).<sup>[9,10]</sup> Therefore, stem cell niches and microenvironment mimicking bio-scaffolds would facilitate the large scale of stem cells' production and specially differentiated cell types preparation.<sup>[11–14]</sup> ECM-mimicking bio-scaffolds apply the effect on cell behavior mainly through physical cues (i.e., stiffness, nanostructured morphologies, charged surfaces, and magnetic field),<sup>[15–19]</sup> and chemical cues (i.e., small chemicals, growth factors, and hormones).<sup>[11,20,21]</sup> Indeed, both physical and chemical cues can efficiently influence IPS cell's functionalities, including regulation of cell adhesion, proliferation, and differentiation. For instance, the change of physical cues could affect cell–cell interactions and trigger the membrane protein activations. In the meantime, the chemical cues could lead


## 1. Introduction

In order to uncover disease mechanisms and develop therapeutic strategies for brain damages and related neurological diseases, developing efficient neural regeneration models is significant and urgent.<sup>[1–5]</sup> As developed neural cells are no longer regenerative and proliferative cells, it is necessary to develop an induced cell line for neural regeneration. Induced pluripotent stem cells

to different integrin activations of cell membranes. The integration of chemical and physical cues utilizing nanostructured scaffolds is fascinating.<sup>[22–28]</sup> However, there is only limited knowledge about regulating the IPS cells' interfacial interactions and the effect on their neural differentiation.

Carbon nanomaterials have been extensively reported in constructing ECM-mimicking scaffolds serving as physical cues in regulating stem cell properties owing to their controllable

Y. Xia, S. Q. Zhou, Prof. R. Haag  
Department of Chemistry and Biochemistry  
Freie Universität Berlin  
Takustrasse 3, 14195 Berlin, Germany  
E-mail: haag@chemie.fu-berlin.de

 The ORCID identification number(s) for the author(s) of this article can be found under <https://doi.org/10.1002/adfm.202010145>.

© 2021 The Authors. Advanced Functional Materials published by Wiley-VCH GmbH. This is an open access article under the terms of the Creative Commons Attribution-NonCommercial License, which permits use, distribution and reproduction in any medium, provided the original work is properly cited and is not used for commercial purposes.

DOI: 10.1002/adfm.202010145

H. Yang  
Institute of Mechanics  
Chair of Continuum Mechanics and Constitutive Theory  
Technische Universität Berlin  
Einsteinufer 5, 10587 Berlin, Germany  
Dr. S. Li  
Department of Chemistry  
Functional Materials  
Technische Universität Berlin  
Hardenbergstraße 40, 10623 Berlin, Germany  
Dr. L. Y. Wang, Dr. Y. J. Tang, Prof. C. Cheng  
College of Polymer Science and Engineering  
State Key Laboratory of Polymer Materials Engineering  
Sichuan University  
Chengdu 610065, China  
E-mail: chong.cheng@scu.edu.cn

nano-topography, high stiffness, and conductivity.<sup>[29–35]</sup> Among diverse carbon nanomaterials, graphene oxide (GO) 2D nanosheets are nanomaterials enriched with carboxyl, hydroxyl, and epoxide groups on the basal platforms, which is significant in improving interactions between GO and proteins via covalent, electrostatic, and hydrogen bonding.<sup>[10,29]</sup> Benefiting from its excellent binding properties to biomolecules, GO played a pivotal role in concentrating soluble chemical cues (growth factors or cytokines, nutrients, and bioactive molecules), which is significant for stem cell growth and differentiation.<sup>[36]</sup> The  $sp^2$  graphitic structures and corresponding large surface area provide an excellent platform for adsorbing bioactive molecules as well, which is sufficient for stem cell fate specification with multiple chemical stimuli.<sup>[37,38]</sup> However, current GO-based neural scaffolds are limited to 2D flat interfaces or nanofibrous composites, and these constructed scaffolds have shown promising promotion of neural differentiation. Nevertheless, the maintaining of stemness, promotion of cellular adhesion, and inhibition of differentiated astrocytes are quite challenging for these currently designed GO-based neural scaffolds. The heparin-mimicking polyanion, hyperbranched polyglycerol sulfates (HPGS), exhibits multivalent, biocompatible, and bio-adhesive polyether backbones. HPGS can serve as a chemical cue for biomedical scaffolds, exhibits outstanding cell-adhesive activities and attachment property toward proteins in the regulation of cell growth and proliferation.<sup>[39,40]</sup> Thus, it is believed that the HPGS functionalized GO-derived scaffolds may provide ideal physical and chemical cues to mediate IPS-cells' stemness and achieve highly efficient neural differentiation.<sup>[11,37,41]</sup>

In this work, we used the multivalent, biocompatible, and bio-adhesive HPGS to modify 2D GO nanosheets to fabricate nano-structured fibrous neural scaffolds with combined physical and chemical cues to mediate the IPS cells' proliferation and lineage specification. First, the GO-HPGS nanosheets were prepared by covalently grafting HPGS on GO. Then 2D nanosheets were coated onto the plasma-treated electrospinning polycaprolactone (PCL) nanofibrous scaffolds, namely, PCL-GO-HPGS. The electrospinning PCL scaffold is biocompatible, degradable, and tunable orientation to mimic the ECM architecture. After coated with GO-HPGS nanosheet, the PCL-GO-HPGS presented an ECM-mimicking porous structure for adequate nutrients and wastes exchanges and integrated physical and chemical cues. Our results suggest that the GO-HPGS modified scaffolds could improve the adhesion and proliferation of IPS cells combined with high efficiency in maintaining their stemness. During the neural differentiation process, the scaffolds could promote neural differentiation and their maturity and meanwhile decrease the lineage specification toward astrocyte. Overall, this study provides a new multivalent/bioadhesive nanofibrous scaffolds for neural regeneration, which integrate the chemical and physical cues to facilitate the targeted differentiation of IPS cells. Furthermore, our design on 2D nanosheet functionalized nanofibrous stem cell-based scaffolds may also provide a new pathway for the fabrication of carbon nanomaterials composites in regenerative therapies as well.

## 2. Results and Discussion

The HPGS, an extracellular-matrix/heparin-mimetic structure, shows intense multivalent interactions with different proteins

and biomolecules, which is crucial in a series of processes, including the adhesion of proteins, recognition of membranes, and signaling processes in cells.<sup>[42–45]</sup> To improve the carbon-to-substrate and carbon-to-carbon interactions, HPGS was directly grafted onto GO nanosheets. Thus, it is believed that the HPGS-modified GO could be used as bio-adhesive and biocompatible nanosheets for the construction of ECM-mimicking scaffolds. As shown in **Figure 1a**, the azides-functionalized hyperbranched polyglycerol (HPG- $N_3$ ,  $\approx 11\%$   $N_3$  substitute to OH groups) was grafted onto GO through covalent conjugations between  $sp^2$  carbon bonds on GO and the azide group on HPG- $N_3$  via nitrene cycloaddition reaction at 120 °C. The hydrophobic interactions and hydrogen bonding between the HPG- $N_3$  and planar GO could significantly improve the amount of grafting HPG on GO. The azide-based nitrene cycloaddition reaction offers an extremely fast and stable method for scalable HPG anchoring.

Then, GO-HPG was sulfated to alter antifouling HPG into multivalent, biocompatible, and bioadhesive HPGS, specifically, GO-HPGS nanosheets. As shown in **Figure 1a**, the GO-HPGS nanosheets were sulfated from the GO-HPG through the  $SO_3$ -pyridine complex. As shown in **Figure 1b**, the TEM images suggest the 2D sheet-structure of GO-HPGS, indicating that the high surface/volume ratio property and 2D structure of GO were well maintained. **Figure 1c** shows the element distribution of the GO-HPGS with high-angle annular dark-field scanning transmission electron microscopy (HAADF-STEM). C, O, S, and Na elements were uniformly distributed on the 2D nanosheet according to the HAADF-STEM image and elemental mapping, suggesting that HPGS are homogeneously grafted onto GO. **Figure 1d** exhibits the atomic force microscope (AFM) picture for pristine GO-HPGS on freshly cleaved mica. The height distribution in **Figure 1e** suggests the difference between the two arrows was about 4.11 nm. **Figure 1f** suggests the calculated thickness distribution of GO-HPGS from 25 nanosheets, and each thickness ranges from 3.9 to 4.3 nm. Meanwhile, the calculated thickness distribution of GO (**Figure S1**, Supporting Information, 0.9 to 1.2 nm) and GO-HPG (**Figure S2**, Supporting Information, 2.3 to 2.5 nm) from 25 nanosheets verifies uniform grafting of HPGS on GO nanosheet.

The Fourier-transform infrared spectroscopy (FTIR) (**Figure S3**, Supporting Information) peaks at 3401.8 (–OH), 3070.1, 2877.2 (–CH–, –CH<sub>2</sub>–), 2106.1 (–N<sub>3</sub>), 1716.3, 1611.2, 1194.6 (C–O), 1022.0, 929.5 (–SO<sub>3</sub>–)  $cm^{-1}$  verified the chemical structure of GO-HPGS. GO-HPGS was further characterized by X-ray photoelectron spectroscopy (XPS, **Figure 1g–i**). **Figure 1g** shows the existence of sulfur element (sulfate groups) and nitrogen element (conjugated azide) on GO-HPGS nanosheets, which verified the successful grafting of HPG- $N_3$  on the planar GO. The high-resolution spectra of C1s (**Figure 1h**) for GO-HPGS indicated the existence of C=C, C–C, C–N, C–O, and C=O peaks. The high-resolution N1s spectra (**Figure 1i**) show three major nitrogen peaks including 401.7 eV ( $=N^+=$  in residual  $N_3$  groups), 400.8 eV ( $-N=$  and  $=N^-$  in residual  $N_3$  groups), and 399.7 eV (cycloaddition-formed N-graphene conjugation).

As an amphiphilic carbon nanomaterial, GO is quite promising for functional nerve repair.<sup>[29]</sup> GO has a high adsorption ability on growth factors and diverse nutrition proteins through the provision of beneficial chemical cues, which could improve

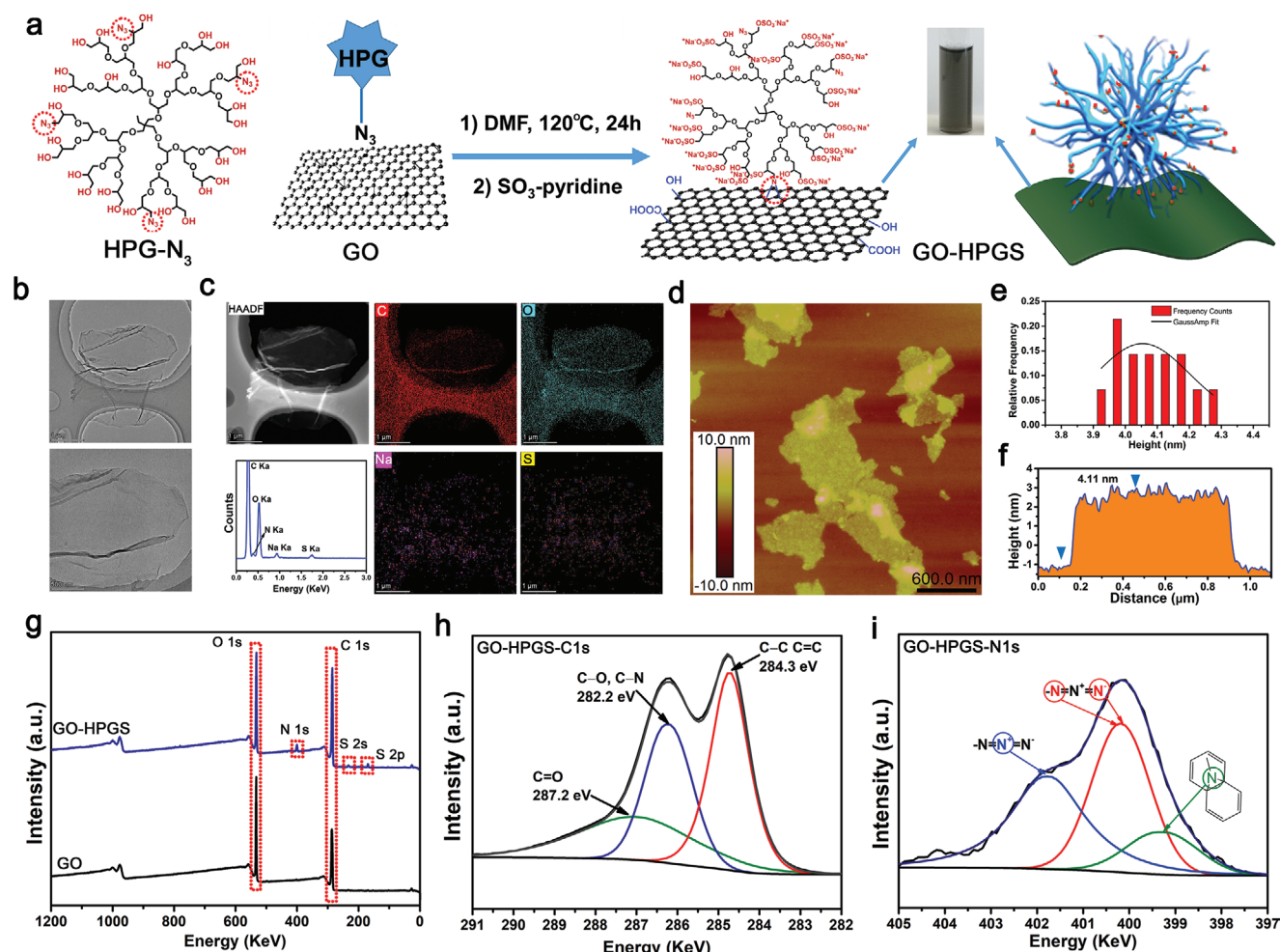


**Figure 1.** a) Scheme of the preparation process of 2D nanosheets by utilizing the GO and HPG-azide through nitrene cycloaddition reaction. b) Typical TEM image of the prepared GO-HPGS nanosheets at different magnifications. c) HAADF-STEM image, EDS curves, and corresponding elemental mapping of the GO-HPGS nanosheets, which revealed the distribution of C, O, Na, and S. d) Representative AFM images of GO-HPGS. e) The calculated thickness distribution of GO-HPGS from 25 nanosheets. Each thickness ranged from 3.9 to 4.3 nm, which indicated the obtained GO-HPGS nanosheets were purely single-layer products. f) The cross section analyses of GO-HPGS and the height difference between the two arrows were about 4.11 nm. g) XPS survey scanning spectra for the GO and GO-HPGS, which is corresponding to sulfur and nitrogen. The high-resolution XPS for h) C1s spectra and i) N1s spectra for GO-HPGS.

the attachment and spread of IPS cells.<sup>[36]</sup> Moreover, due to the hierarchical structures of fibrous neural scaffolds on the microscale and nanoscale, the fibrous scaffolds provide physical cues for neural tissues to adhere and grow. In this work, with the coating of GO-HPGS nanosheets, the nanostructured fibrous scaffold was constructed to offer an appropriate micro-environment for IPS cells' survival and differentiation. The PCL was chosen as the electrospinning matrix to build the original fibrous scaffold due to its well-established biocompatible and degradable property, which is pivotal for biomedical applications. **Figure 2a** exhibits that a syringe with a metal needle was filled with PCL solution, after being applied with a 16 kV high voltage; the solution was split into fibers and fall onto a rotating drum collector. Then, the fibrous scaffolds were treated with 1 min of O<sub>2</sub> plasma to generate radicals on the fiber's surface. Then 1 mg mL<sup>-1</sup> HPGs, GO, and GO-HPGS aqueous solutions were dipped into the plasma-treated fiber mats to prepare the PCL-HPGS, PCL-GO, and PCL-GO-HPGS scaffolds, respectively.

**Figure 2b** shows the morphologies of the scaffolds under scanning electron microscopy (SEM). The electrospinning PCL fiber mats (≈50 μm in thickness) composed of crossing fibers with a diameter of around 1 μm. According to the amplified SEM image, the GO and GO-HPGS nanosheets-coated samples had corrugations on the fiber's surface compared to the smooth surface of the original PCL fiber. This suggested that the GO and GO-HPGS 2D thin-films were tightly wrapped around the fiber's surface, and a 3D nanofibrous structure could be well-maintained. The energy dispersive spectrometer data (EDS) and element mapping on PCL-GO-HPGS (**Figure 2c**; **Figure S7**, Supporting Information) indicated the existence of sulfur due to the coating of GO-HPGS. The FTIR data in **Figure 2d** gives the characteristic peaks for different samples, respectively. There are -OH and -SO<sub>3</sub>- peaks on PCL-HPGS, -OH peaks on PCL-GO, and -OH, -N<sub>3</sub>, and -SO<sub>3</sub>- peaks on PCL-GO-HPGS, which verified the successful coating of the above samples. The water contact angle (**Figure 2e**) on pure

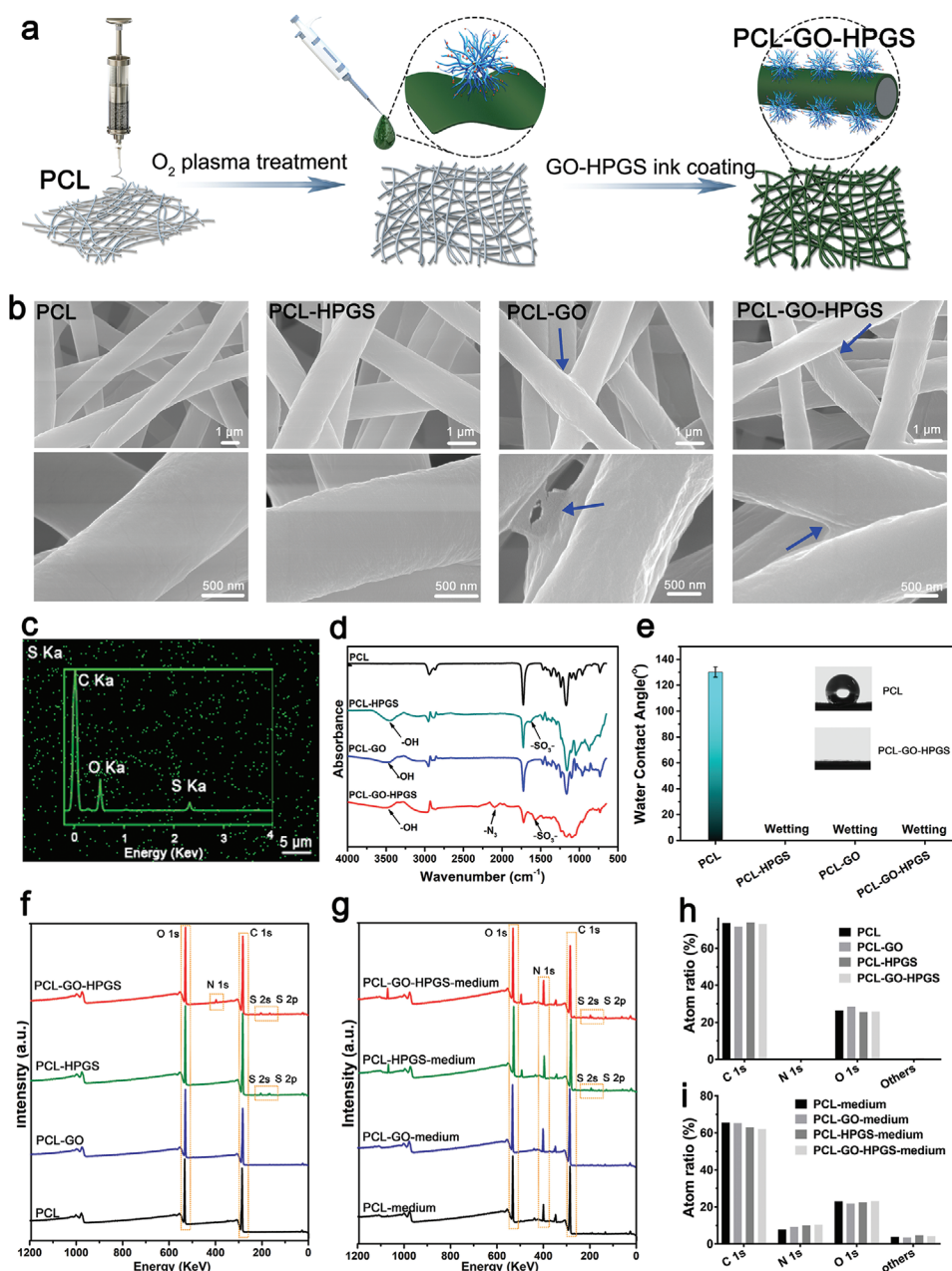


**Figure 2.** a) Schematic images for the electrospinning process of PCL fibers and coating process of GO-HPGS nanosheets. b) SEM pictures of PCL, PCL-HPGS, PCL-GO, and PCL-GO-HPGS samples. The nanosheets are marked with blue arrows. c) The SEM element mapping and EDS curves of the S element on PCL-GO-HPGS. d) FTIR spectra for bare and nanosheet-coated PCL fibrous scaffolds. e) The average static water contact angle of bare, nanosheet-coated PCL fibrous scaffolds. XPS spectra for f) fibrous scaffolds and g) medium-immersed fibrous scaffolds. h) The atom percentages of C, N, O, and others on fibrous scaffolds and i) medium-immersed fibrous scaffolds.

PCL is around 129°. After coating with different samples, the surface was transferred to hydrophilic. As shown in Figure 2f, Table 1 and Tables S1,S2, Supporting Information, XPS has been further characterized to verify the successful coating of 2D nanosheets onto PCL nanofibers. According to the XPS survey scanning spectra in Figure 2f, there exists abundant sulfur element on the PCL-HPGS fibers, and nitrogen and sulfur elements on PCL-GO-HPGS fibers, thus suggesting that HPGS and GO-HPGS nanosheets were coated onto PCL fiber,

respectively. As shown in Figure 2g,i, the contents of element N1s on samples (after immersion in a cell culture medium) increased compared to that in Figure 2f,h. Accordingly, it is indicated that these scaffolds could absorb molecules of amino acids based peptides or proteins from the cell culture media, which is critical for the regulation and specification of IPS cells' growth and differentiation. After being coated with GO-HPGS nanosheets, the scaffolds exhibited much better absorption ability toward the amino acids based peptides/proteins

**Table 1.** The surface atomic percentage of the 2D nanosheet-coated PCL fibers with/without immersion of media. The data is according to XPS results.

Sample	C1s [%]	O1s [%]	N1s [%]	S2p [%]	Others
PCL	73.58	26.42	–	–	–
PCL-HPGS	74.11	25.64	–	0.24	–
PCL-GO	71.82	28.18	–	–	–
PCL-GO-HPGS	73.46	25.85	0.48	0.21	–
PCL-medium	64.50	22.99	8.78	0.34	3.39
PCL-HPGS-medium	65.37	21.84	9.32	0.40	3.07
PCL-GO-medium	63.30	22.41	9.98	0.31	4.00
PCL-GO-HPGS-medium	62.17	23.17	10.43	0.41	3.82

and other small molecules, which could be further employed to manipulate the IPS cells' fates. Meanwhile, the cyclic voltammetry curves (Figure S8, Supporting Information) show that the PCL-GO-HPGS coated scaffolds present the best electrochemical activity in PBS buffer compared to the bare PCL and PCL-GO, which can be attributed to the incorporation of  $\text{SO}_3^-$  groups.

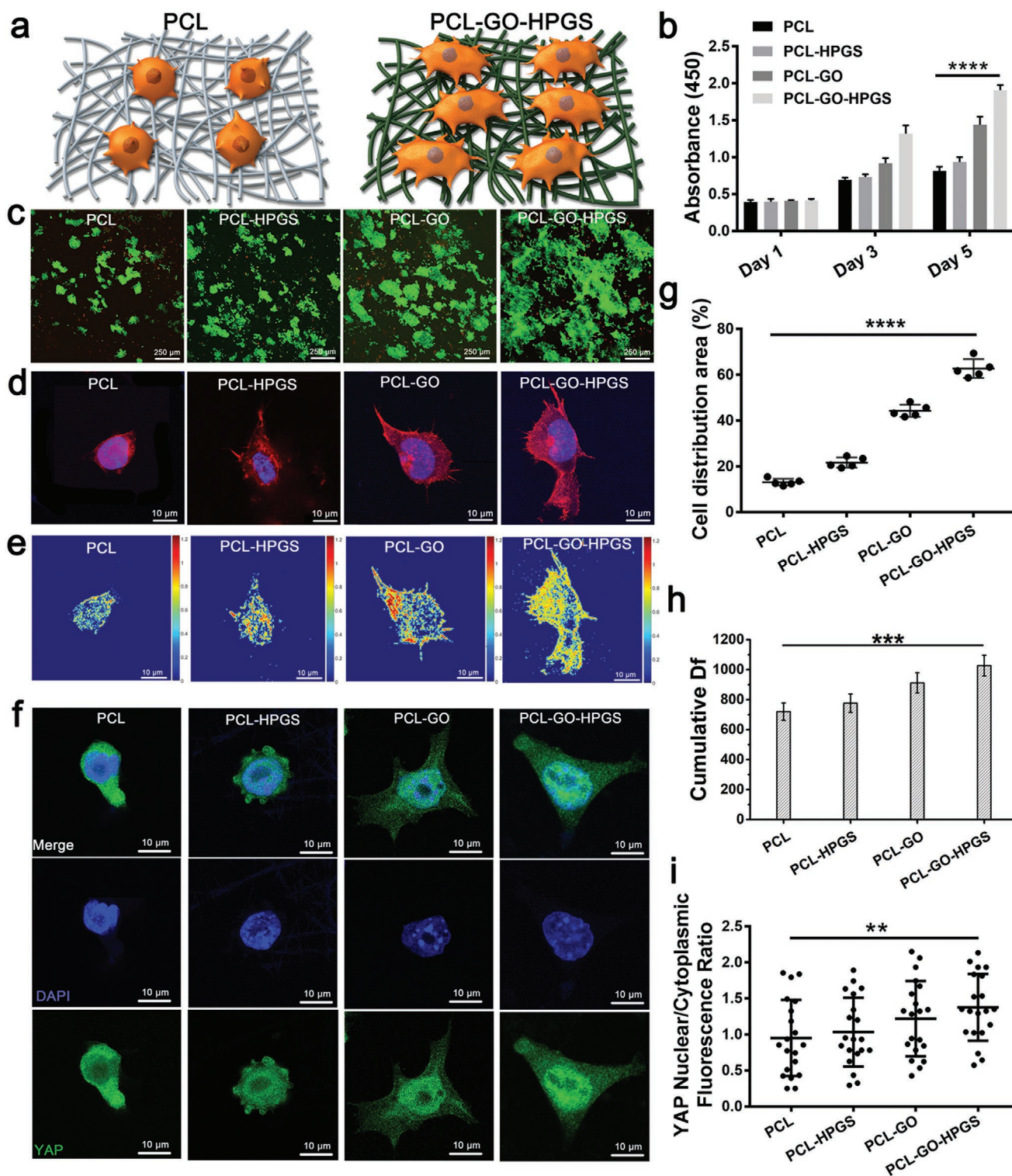
To evaluate whether the GO-HPGS nanosheets coated scaffolds are suitable for stem cell-related neural regeneration, the IPS cells were chosen to observe cell viability, adhesion, and proliferation, when grown on different nanofibrous scaffolds. **Figure 3a** shows the schematic image of cell adhesion properties on PCL and GO-HPGS nanosheet-coated scaffolds. After 1, 3, and 5 days of culture, the CCK-8 assay kit was utilized to evaluate the IPS cell proliferation rate on nanofibrous scaffolds (Figure 3b). After 5 days' culture, cells that proliferated on the GO-HPGS nanosheet-coated scaffolds were around twofold as much as that on PCL. The cells on PCL-GO and PCL-HPGS proliferated better than that on PCL as well, which indicated that the coating of GO and HPGS could both promote the proliferation of IPS cells. The Live/dead cell staining (Figure 3b) on PCL-GO-HPGS on day 3 shows homogeneous and interconnected cells, which was much better than the PCL-GO, PCL-HPGS, and bare PCL, indicating that GO and HPGS had synergistic improvement effect for the growth and proliferation of IPS cells. The lack of bioactive chemical ligands and relatively smooth fiber surface led to poor cell adherence and growth on bare PCL. ECM preserve IPS cells in the niche or assists in starting signal transduction, while the surface coating of GO-HPGS concentrates soluble growth factors or cytokines, which regulates stem cell fate via immobilizing signaling molecules and creating cytokine gradients.<sup>[12]</sup>

To investigate the interactions of GO-HPGS-coated fibers with IPS cells, the cell nuclear was stained with DAPI (blue), and the F-actin was stained with phalloidin (red), then the fluorescent images were observed with confocal microscopy. **Figure 3d** shows that cells grown on PCL-GO-HPGS had much more cell pseudopodium on the surface, suggesting more binding sites for IPS cells to adhere. 2D fractal dimensions (Df) are a dimensionless value in quantifying the complexity of spatial arrangement and complexity for the cell cytoskeleton. MATLAB was utilized to analyze the corresponding Df (Figure 3e) according to F-actin staining. The higher cytoskeleton complexity on GO-HPGS nanosheet-coated surface

indicated that the cells have much more adhesion spots due to the corrugations on the GO-coated structure and the multivalent HPGS's protein binding affinity. The quantitative Df values of whole-cell spheroids on PCL-GO-HPGS were gradually bigger than the PCL-GO, PCL-HPGS, and bare PCL (Figure 3h). Furthermore, correlative analysis of the cell area showed that the cell-spreading area on GO-HPGS nanosheets coated surface was larger than those on bare PCL, suggesting more anchoring opportunities for cells to facilitate cell motility and adhesion. In general, after the characterization of IPS cells' viability, proliferation, adhesion, and spreading, results indicated that the GO-HPGS-coated fibrous scaffolds achieved significant progress in providing an excellent environment for fragile IPS cells to survive.

During the cell adhesion and spreading process, the rearrangement of the actin cytoskeleton would regulate cellular signaling pathways change.<sup>[46]</sup> Increased cell spreading is frequently accompanied by yes associate protein (YAP) relocation and following YAP-responsive gene transcription activation.<sup>[46]</sup> Its localization in nuclei results in IPS cells could promote cell proliferation.<sup>[47,48]</sup> Meanwhile, activated YAP nuclear translocation could mediate stemness maintenance in IPS cells.<sup>[49,50]</sup> Thus, we further investigated the YAP signal on PCL, PCL-HPGS, PCL-GO, and PCL-GO-HPGS using immunofluorescence staining (Figure 3f; Figure S10, Supporting Information). It is evident that YAP was located in the cytoplasm on PCL, however, more YAP signals exist in nucleus on PCL-GO-HPGS. The YAP nuclear/cytoplasm ratio in Figure 3i also suggests that more YAP is activated into nucleus on PCL-GO-HPGS, which proves that PCL-GO-HPGS could promote IPS cells proliferation and promote the stem cell stemness.

Nanog, Sox2, OCT4, and SSEA1 are transcription factors that are pivotal to preserve the stemness of undifferentiated IPS cells, which are involved in the regulation of self-renewal development and the determination of cell fate.<sup>[49,51]</sup> To better indicate the primitiveness and stemness of the reprogrammed cells, we observed the colonies that stained positive for four primitive stem cell markers, Nanog, Sox2, OCT4, and SSEA1, on day 3 after being cultured in a growth medium (**Figure 4a,b**). The colony, which was grown on PCL-HPGS, PCL-GO, and PCL-GO-HPGS, was larger than that on PCL, which indicated that HPGS and GO could both promote IPSC proliferation. The relative fluorescence intensities in Figure 4e,f suggests that the PCL-GO-HPGS scaffolds could preserve the stemness very well and even slightly better than pure PCL. The stemness-marker fluorescence intensity of the colonies was consistent with the result of YAP nuclear translocation. The reason could be attributed to the PCL-GO-HPGS scaffold's good adsorption of protein (including the differentiation inhibitor) from the growth medium. **Figure 4c** represents the intensity distribution profiles of Nanog and Sox2 from the center to the edge of the cell colonies grown on PCL, PCL-HPGS, PCL-GO, and PCL-GO-HPGS. **Figure 4f** represents OCT4 and SSEA1 on scaffolds, respectively. The colony radius for PCL is around 80  $\mu\text{m}$ , and PCL-GO-HPGS is around 120  $\mu\text{m}$ . Meanwhile, the fluorescence intensity at the edge of the colony was relatively stronger than that in the center, which means that the outer cells could absorb more inhibitors from the medium and preserve the stemness better



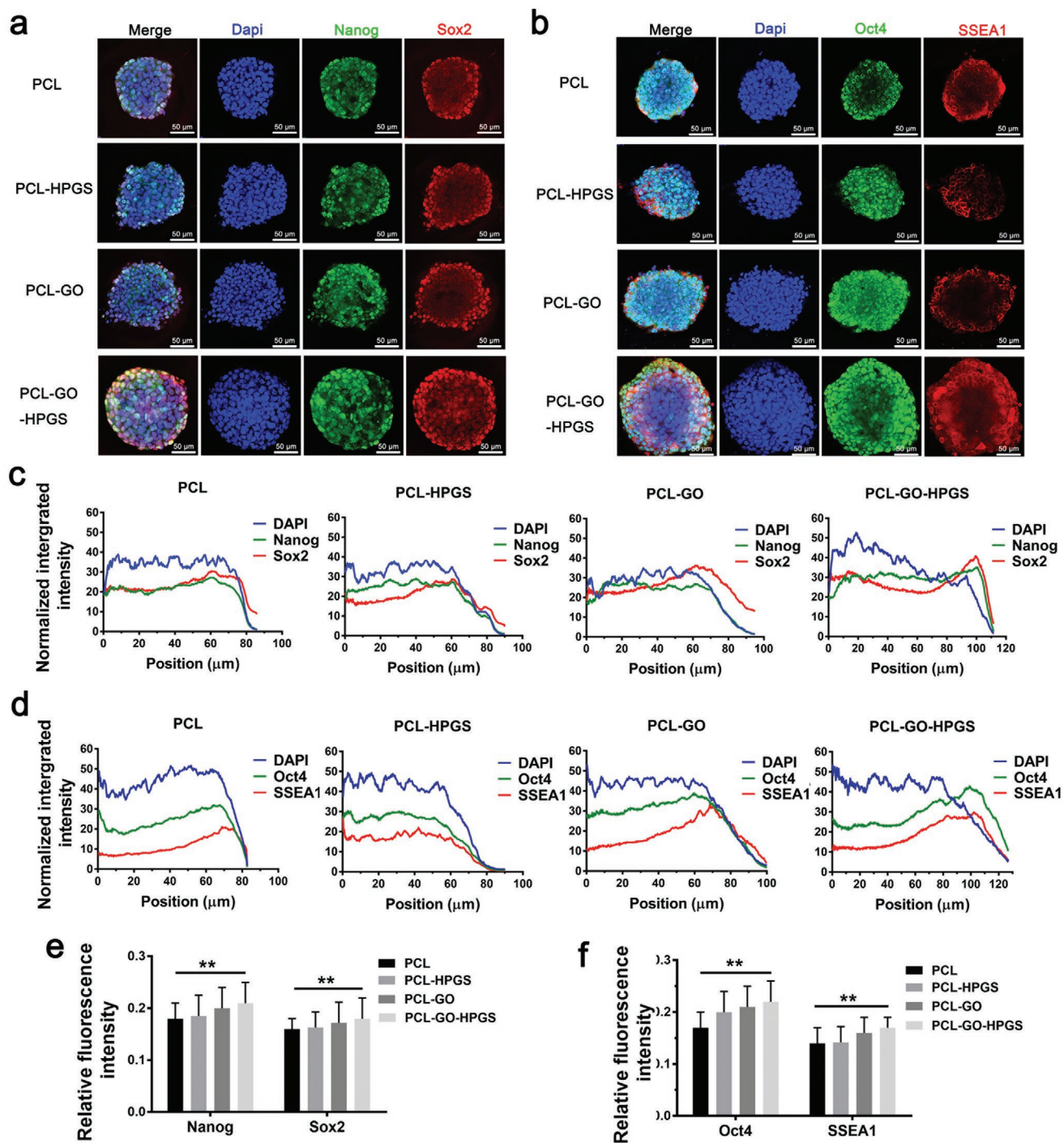


**Figure 4.** Representative immunofluorescence staining of stemness markers a) Nanog (green) and Sox2 (red); b) Oct4 (green) and SSEA1 (red) for IPS cells on scaffolds. Respective intensity distribution profiles of c) Nanog and Sox2, d) Oct4 and SSEA1 from the center to the edge of the cell colonies grown on scaffolds, respectively. Quantitative analysis for grey intensity of immunofluorescence-stained images to get the average expressions of e) Nanog and Sox2 and f) Oct4 and SSEA1. ( $n = 30$ ),  $***p < 0.001$ ,  $**p < 0.01$ , and  $*p < 0.05$ .

in the growth medium. The colony edge signal on GO-HPGS nanosheet-coated scaffolds was more extensive than that on bare PCL, indicating that GO-HPGS may have accumulated differentiation inhibitors from cell culture media to promote the stemness of IPS cells.

As shown in **Figure 5a**, the embryonic body was prepared and seeded on nanofibrous scaffolds and then developed toward neurites. As a kind of intermediate filament protein, Nestin is frequently expressed in nerve cells, which is quite often used in dividing cells during the early stages of

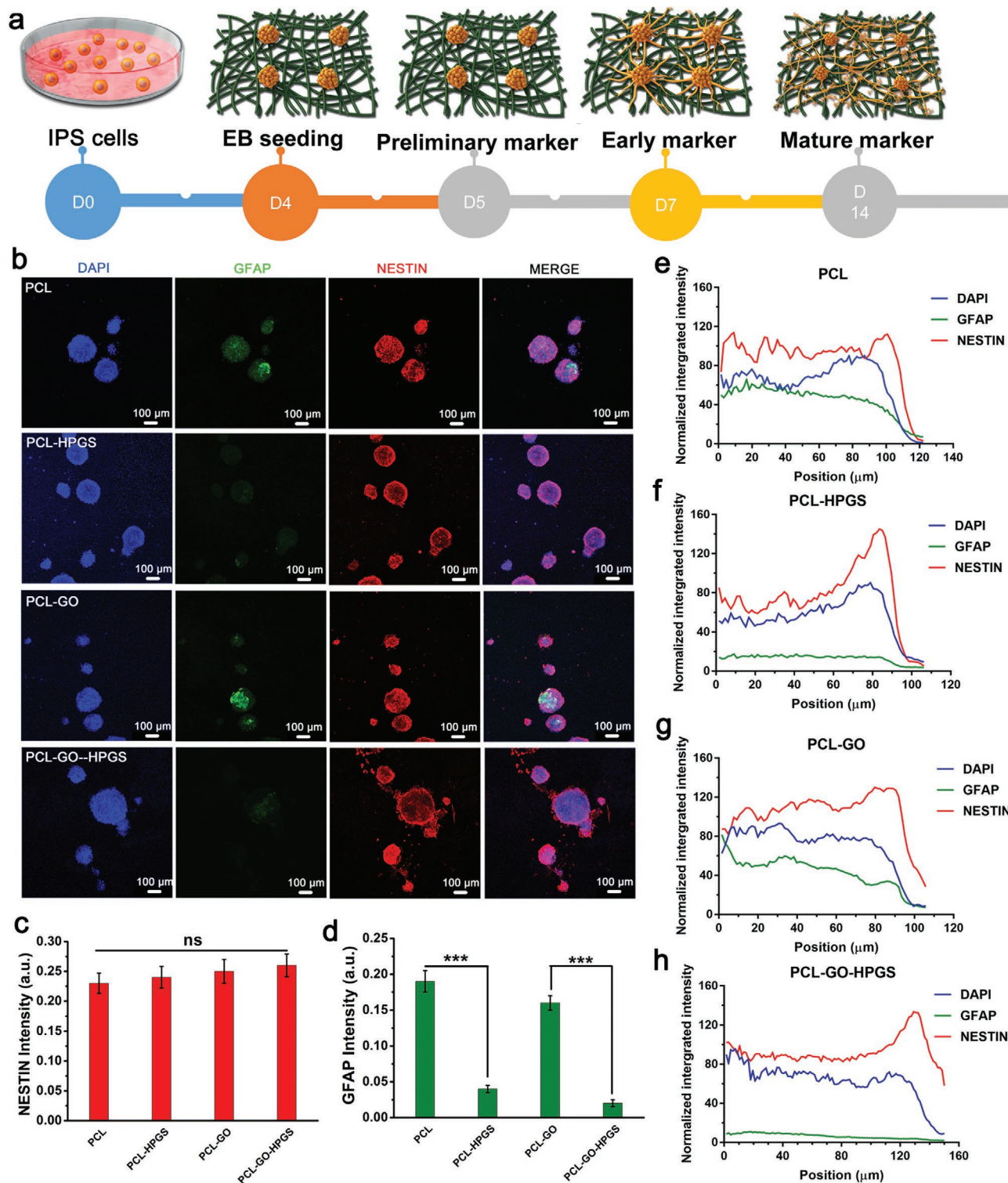


**Figure 5.** a) Schematic timeline of the preparation of embryoid bodies (EBs) and the neural differentiation of IPS cells. b) Immunofluorescence staining of primary neuron marker GFAP and Nestin (blue, DAPI; green GFAP; red Nestin) at 5 days. The average expressions of c) Nestin and d) GFAP were quantitatively analyzed from the immunofluorescence-stained images' grey intensity, respectively. Respective intensity distribution profiles of GFAP and Nestin from the center to the edge of the EB grown on e) PCL, f) PCL-HPGS, g) PCL-GO, and h) PCL-GO-HPGS, respectively. ( $n = 10$ ). \*\*\* $p < 0.001$ , \*\* $p < 0.01$ , and \* $p < 0.05$ .



development in the radial growth of the axon.<sup>[52,53]</sup> As the same family of intermediate filament protein in the central nerve system, glial fibrillary acidic protein (GFAP) is expressed mostly in astrocytes and ependymal cells.<sup>[54]</sup> To study IPS cells' differentiation process on different scaffolds, the GFAP and Nestin were stained and observed after 5 days of culture in the neural differentiation medium (Figure 5b). There were only seeded embryonic bodies on all scaffolds, and no obvious neurites and axons could be observed. Nestin's relative fluorescence intensity analysis in Figure 5c suggests no significant difference between bare PCL and GO-HPGS-coated scaffolds as for the average expression of Nestin. However, when we compared the GFAP expression in Figure 5d, the evolution process toward astrocyte was mainly confined to PCL and PCL-GO. The displayed increased astrocytes could diminish glutamate transporter current and may be detrimental to neurons and axons' development.<sup>[54]</sup> Figure 5e–h represents the intensity distribution profiles of GFAP and Nestin from the center to the edge of the embryonic body grown on PCL, PCL-HPGS, PCL-GO, and PCL-GO-HPGS, respectively. The embryonic body radius ranges from 40 to 110  $\mu\text{m}$ . Meanwhile, the fluorescence intensity for the red Nestin at the edge of the colony was more potent than that in the center, which means that the outward cells could absorb more differentiation factors and hormones from the medium. However, the distribution and levels of GFAP signal on PCL-HPGS and PCL-GO-HPGS were quite low, which suggests that the successful coating of HPGS could inhibit the expression of GFAP and then prevent the differentiation potential to astrocyte.

To further evaluate the neural differentiation activities after the embryonic bodies were seeded on GO-HPGS-nanosheet-coated samples. III  $\beta$ -tubulin (Tuj1), as an early neural marker, was investigated. As an exclusively expressed in neurons microtubule component, Tuj1 stands for regenerated axons and neurofilaments.<sup>[55,56]</sup> Figure 6a exhibits immunofluorescence photo of earlier neuron marker protein Tuj1, corresponding 2D Df, and fluorescence intensity maps after 7 days of culture according to the process in Figure 6a and Figures S11, S12, Supporting Information. The immunostaining picture shows a higher neuron differentiation rate and a more prolonged axon on PCL-GO-HPGS than other samples. These neurites, which were spread out very well on PCL, PCL-HPGS, PCL-GO, and PCL-GO-HPGS fibrous structures, were easy to recognize. The statistical analysis of neurites distribution in Figure 6b suggests the PCL-GO-HPGS surface could promote the elongation of neurites. After MATLAB analysis, according to the Tuj1 staining, 2D Df and fluorescence intensity map were obtained, which proved that the neurites adhere and elongate quite well on the GO-HPGS nanosheet-coated scaffolds. They also had denser and longer neurites compared with bare PCL scaffolds. The neurite intersections indicated the apical node and spines of the neurites.

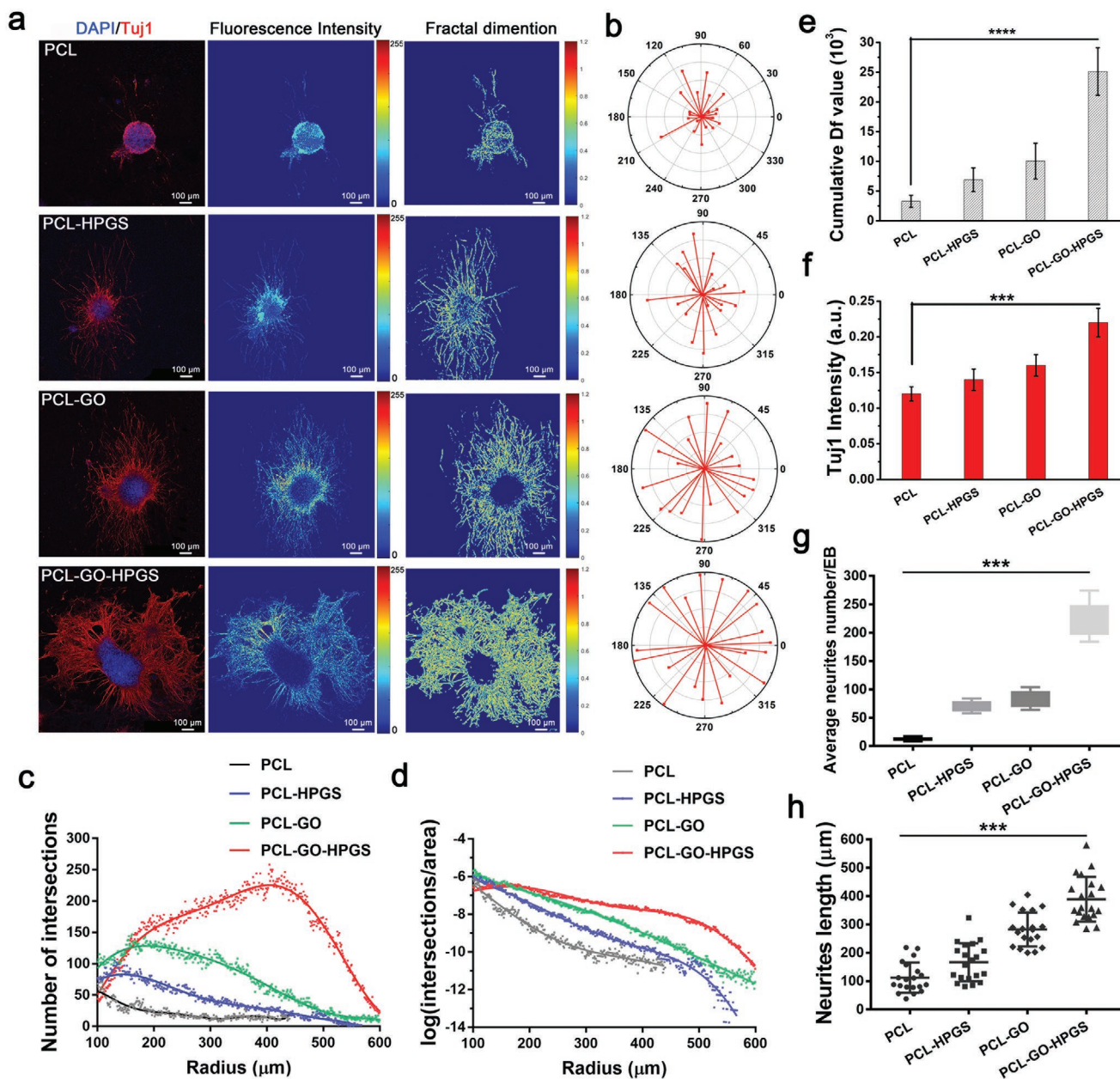
To investigate the number and distribution of spines, the neurite intersections' changes from the EB center to the edge were investigated using image J (Figure 6c). The number of intersections on PCL-GO-HPGS was around 5 times compared with bare PCL. Meanwhile, the intersection number increased from radius 100–400  $\mu\text{m}$  and then decreased to the edge. The number of neurites intersections per area in

Figure 6d also suggests that PCL-GO-HPGS had the largest number of apical nodes and spines along with the change from the EB center to the edge. The Df values in Figure 6e suggest the quantification of neurites' spatial arrangement. The neurites on GO-HPGS nanosheet-coated scaffolds have a higher spatial arrangement complexity, for example, branches' types and branches' amounts. As shown in Figure 6f, the relative expression level of Tuj1 on PCL is only half of that on PCL-GO-HPGS. The average neurite number per EB on PCL-GO-HPGS ( $232 \pm 52$ ) was much more massive than that on bare PCL ( $12 \pm 10$ ) (Figure 6g). Besides, the neurite length changed from PCL ( $101 \pm 34 \mu\text{m}$ ) to PCL-GO-HPGS ( $345 \pm 109 \mu\text{m}$ ), which verified that the GO-HPGS nanosheets' coating could significantly improve neurite elongation in vitro.

As we established a timeline differentiation process for IPS cells from EBs to neural cells, IPS cells were cultured in a suspension of medium to form EBs enriched with neural progenitors. The subsequent adherent culture of EBs on scaffolds resulted in the generation of Tuj1-positive immature neurons at day 5–7, and these cells were then differentiated into mature neurons with increased positivity for NeuN and microtubule-associated protein 2 (MAP2) after 1 week.<sup>[57]</sup> NeuN is a protein mainly expressed in neural nuclei, and MAP2 is a pivotal microtubule protein during the neuritogenesis-microtubule assembly process.<sup>[58]</sup> Figure 7a exhibits a few axonal/microtubule sprouting after 14 days of differentiation on bare PCL. However, well-grown neural microtubules and microfilaments could be observed spreading on GO-HPGS nanosheet-coated scaffolds, suggesting that GO-HPGS nanosheets could promote mature neurites' formation. The relative fluorescence intensity in Figure 7c indicates the increased average NeuN and MAP2 expression on PCL-GO-HPGS scaffolds. The fluorescence co-localization analysis in Figure 7b suggests the distribution of MAP2 (red) and NeuN (green) signals in fluorescence microscopy images, which can be used to determine whether two probes co-distributed with one another.<sup>[59]</sup> It is evident that the distribution of red signal and green signal on PCL-GO-HPGS was most discrete, which is in line with the Manders' co-localization coefficients (MCC) in Figure 7d and Pearson's correlation coefficient (PCC) in Figure 7e. The smaller the value of the coefficient means the less co-localization is related. Since NeuN protein was mainly expressed in the nuclear, the less co-localization of MAP2 with NeuN on PCL-GO-HPGS suggests more expression of MAP2 in axonal microtubule, which proved more mature neurites on PCL-GO-HPGS than on bare PCL.

### 3. Conclusion

In summary, we have prepared a biocompatible and multi-valent polyanion to modify the GO to obtain bioadhesive 2D nanosheets and the 2D nanosheet-coated nanofibrous scaffolds, which exhibited combined physical and chemical cues to promote IPS cells toward neural differentiation. The prepared ECM-mimicking PCL-GO-HPGS scaffolds exhibited high efficiency in promoting the IPS cells' adhesion and proliferation, the unique advantages has been compared in Table S3, Supporting Information. Meanwhile, the PCL-GO-HPGS



**Figure 6.** a) The confocal image for earlier neuron marker protein, Tuj1 (blue, DAPI; red, Tuj1), the corresponding 2D fractal dimension (Df) and fluorescence intensity map after 7 days of culture. b) Top 20 long axons on each sample, the radius, and  $\theta$  ( $^\circ$ ) define the length and the angle of the axons, respectively. c) The number of neurites' intersections along with the change from the EB center to the edge. Neurite intersections indicated the apical node and spines of the neurites. d) The number of neurite intersections per area along with the change from the EB center to the edge. e) The analysis of the quantitative cumulative Df value within a single cell on different samples ( $n = 20$ ). f) Quantitative analysis, according to the grey intensity, results in the average expression of  $\beta$ III tubulin (Tuj1). g) The average neurites number per EB on different samples ( $n = 20$ ). h) The neurite length distribution of different samples ( $n = 20$ ). \*\*\* $p < 0.001$ , \*\* $p < 0.01$ , and \* $p < 0.05$ .

scaffolds could keep the seed IPS cells in a good stemness state in the growth medium. Furthermore, we have also validated that the introduced HPGS on the scaffold surface could decrease the differentiation chance toward astrocyte, and GO coating could promote the neural differentiation efficiency and maturity. Benefiting from both advantages of HPGS and GO, the scaffolds could promote neural differentiation and decrease the lineage specification toward astrocytes.

Overall, this study provides a new strategy to design multi-valent/bioadhesive nanofibrous scaffolds for neural regeneration, which integrates the chemical and physical cues to facilitate the targeted differentiation of IPS cells. Our design on 2D nanosheet functionalized nanofibrous stem cell-based scaffolds may also provide a new pathway for the fabrication of carbon nanomaterials-based biocomposites in regenerative therapies as well.

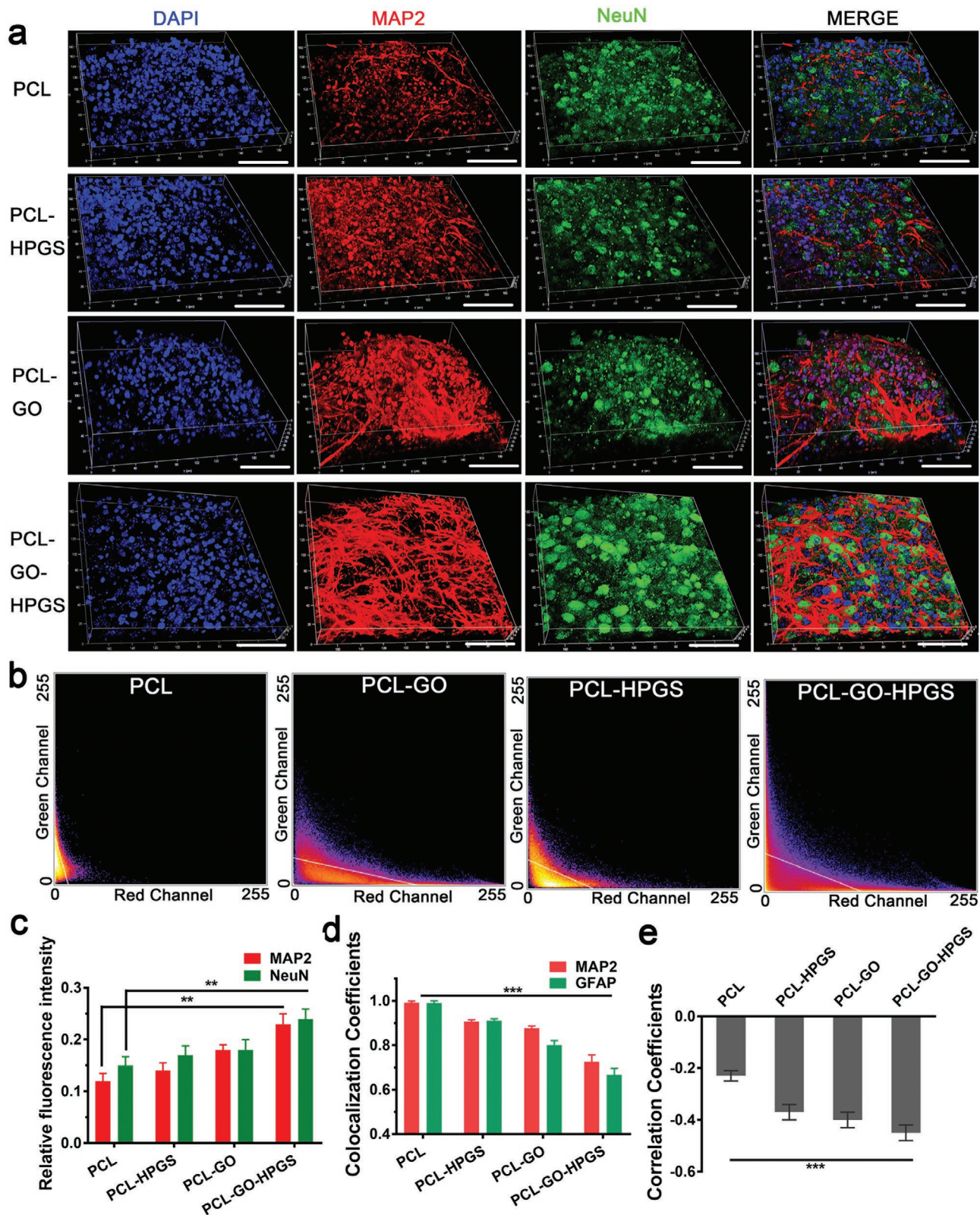


**Figure 7.** a) Confocal image of mature neuron marker protein NeuN and MAP2 at day 14 on different samples (blue, DAPI; green, NeuN; red, MAP2), the scale bar is 50  $\mu\text{m}$ . b) The co-localization map of NeuN and MAP2 protein, which is according to (a). c) The quantitative intensity of NeuN and MAP2 according to the immunofluorescence-stained images. d) MCC of MAP2 and NeuN, MCC is the percentage of co-localized protein in the total expressed protein. e) PCC of MAP2 and NeuN protein, the smaller the value, the less co-localization related.  $***p < 0.001$ ,  $**p < 0.01$ , and  $*p < 0.05$ .

## 4. Experimental Section

Materials, preparation, and characterization of methods, stem cell culture and staining experiments, and statistical analysis are all shown in the Supporting Information.

## Supporting Information

Supporting Information is available from the Wiley Online Library or from the author.

## Acknowledgements

This work was financially sponsored by the National Key R&D Program of China (2019YFA0110600, 2019YFA0110601), National Natural Science Foundation of China (Nos. 82071938, 82001824, 82001829, 51903178, 81971622, 51803134, and 51703141), and Deutsche Forschungsgemeinschaft (DFG) through grants from the Collaborative Research Center (SFB) 765. Y.X. and S.Z. acknowledge the support from China Scholarship Council (CSC). C.C. acknowledges the support of the State Key Laboratory of Polymer Materials Engineering (Grant No. sklpm2019-2-03), the Science and Technology Project of Sichuan Province (Nos. 18YJC1417, 2020YFH0087, 2019YFS0219, and 2020YJ0055), Fundamental Research Funds for the Central Universities, Thousand Youth Talents Plan, Alexander von Humboldt Fellowship, and DRS POINT Fellowship. Dr. Pamela Winchester is sincerely acknowledged for language polishing the manuscript. The authors would like to acknowledge the assistance of the Core Facility BioSupraMol at the Freie Universität Berlin supported by the DFG and Zhongkebaice Technology Service Co. Ltd. Beijing, China, for materials characterizations. The authors are also thankful for the help of Dr. Mi Zhou, Dr. Chao He, Dr. Lang Ma, and Prof. Hongrong Luo at Sichuan University.

Open access funding enabled and organized by Projekt DEAL.

## Conflict of Interest

The authors declare no conflict of interest.

## Data Availability Statement

Research data are not shared.

## Keywords

bio-adhesive graphene nanostructures, multivalent polyanions, nanofibrous scaffolds, neural differentiation, stem cell regeneration

Received: November 25, 2020

Revised: February 16, 2021

Published online: March 10, 2021

[1] R. G. Canter, J. Penney, L.-H. Tsai, *Nature* **2016**, 539, 187.

[2] B. De Strooper, E. Karran, *Cell* **2016**, 164, 603.

[3] L. A. Rocha, D. Silva, S. Barata-Antunes, H. Cavaleiro, E. D. Gomes, N. A. Silva, A. J. Salgado, *Adv. Funct. Mater.* **2020**, 30, 1909083.

[4] M. J. Landry, K. Gu, S. N. Harris, L. Al-Alwan, L. Gutsin, D. De Biasio, B. Jiang, D. S. Nakamura, T. C. Corkery, T. E. Kennedy, C. J. Barrett, *Macromol. Biosci.* **2019**, 19, 1900036.

- [5] Q. Tang, S. Cao, T. Ma, X. Xiang, H. Luo, P. Borovskikh, R. D. Rodriguez, Q. Guo, L. Qiu, C. Cheng, *Adv. Funct. Mater.* **2021**, 31, 2007475.
- [6] K. J. Brennan, A. Simone, J. Jou, C. Gelboin-Burkhardt, N. Tran, S. Sangar, Y. Li, Y. Mu, G. Chen, D. Yu, S. McCarthy, J. Sebat, F. H. Gage, *Nature* **2011**, 473, 221.
- [7] G. Lee, E. P. Papapetrou, H. Kim, S. M. Chambers, M. J. Tomishima, C. A. Fasano, Y. M. Ganat, J. Menon, F. Shimizu, A. Viale, V. Tabar, M. Sadelain, L. Studer, *Nature* **2009**, 461, 402.
- [8] M. C. N. Marchetto, C. Carron, A. Acab, D. Yu, G. W. Yeo, Y. Mu, G. Chen, F. H. Gage, A. R. Muotri, *Cell* **2010**, 143, 527.
- [9] L. Hou, J. Kim, J. Coller, V. Natu, N. Huang, *Circ. Res.* **2016**, 119, A357.
- [10] M. L. Lovett, T. J. F. Nieland, Y.-T. L. Dingle, D. L. Kaplan, *Adv. Funct. Mater.* **2020**, 30, 1909146.
- [11] A. Higuchi, Q.-D. Ling, Y. Chang, S.-T. Hsu, A. Umezawa, *Chem. Rev.* **2013**, 113, 3297.
- [12] A. Higuchi, Q.-D. Ling, Y.-A. Ko, Y. Chang, A. Umezawa, *Chem. Rev.* **2011**, 111, 3021.
- [13] S. Gao, M. X. Chen, P. Wang, Y. Li, Z. G. Yuan, W. M. Guo, Z. Z. Zhang, X. L. Zhang, X. G. Jing, X. Li, S. Y. Liu, X. Sui, T. F. Xi, Q. Y. Guo, *Acta Biomater.* **2018**, 73, 127.
- [14] X. Sun, Y. Wang, Z. Y. Guo, B. Xiao, Z. Sun, H. Y. Yin, H. Y. Meng, X. Sui, Q. Zhao, Q. Y. Guo, A. Y. Wang, W. J. Xu, S. Y. Liu, Y. J. Li, S. B. Lu, J. Peng, *Adv. Healthcare Mater.* **2018**, 7, 1800276.
- [15] X. Xue, Y. Sun, A. M. Resto-Irizarry, Y. Yuan, K. M. Aw Yong, Y. Zheng, S. Weng, Y. Shao, Y. Chai, L. Studer, J. Fu, *Nat. Mater.* **2018**, 17, 633.
- [16] J. Zhang, C. Cheng, J. L. Cuellar-Camacho, M. Li, Y. Xia, W. Li, R. Haag, *Adv. Funct. Mater.* **2018**, 28, 1804773.
- [17] M. J. Landry, F.-G. Rollet, T. E. Kennedy, C. J. Barrett, *Langmuir* **2018**, 34, 8709.
- [18] H. Chen, J. Sun, Z. Wang, Y. Zhou, Z. Lou, B. Chen, P. Wang, Z. Guo, H. Tang, J. Ma, Y. Xia, N. Gu, F. Zhang, *ACS Appl. Mater. Interfaces* **2018**, 10, 44279.
- [19] Y. Xia, J. Sun, L. Zhao, F. Zhang, X.-J. Liang, Y. Guo, M. D. Weir, M. A. Reynolds, N. Gu, H. H. K. Xu, *Biomaterials* **2018**, 183, 151.
- [20] K. Alberti, R. E. Davey, K. Onishi, S. George, K. Salchert, F. P. Seib, M. Bornhäuser, T. Pompe, A. Nagy, C. Werner, P. W. Zandstra, *Nat. Methods* **2008**, 5, 645.
- [21] M. X. Chen, Z. X. Feng, W. M. Guo, D. J. Yan, S. Gao, Y. Y. Li, S. Shen, Z. G. Yuan, B. Huang, Y. Zhang, M. J. Wang, X. Li, L. B. Hao, J. Peng, S. Y. Liu, Y. X. Zhou, Q. Y. Guo, *ACS Appl. Mater. Interfaces* **2019**, 11, 41626.
- [22] J. Xue, T. Wu, Y. Dai, Y. Xia, *Chem. Rev.* **2019**, 119, 5298.
- [23] J. Xue, T. Wu, J. Li, C. Zhu, Y. Xia, *Angew. Chem., Int. Ed.* **2019**, 58, 3948.
- [24] J. Xue, J. Xie, W. Liu, Y. Xia, *Acc. Chem. Res.* **2017**, 50, 1976.
- [25] J. Xue, C. Zhu, J. Li, H. Li, Y. Xia, *Adv. Funct. Mater.* **2018**, 28, 1705563.
- [26] J. Zhao, W. Cui, *Adv. Fiber Mater.* **2020**, 2, 229.
- [27] J. Zhou, Z. Hu, F. Zabihi, Z. Chen, M. Zhu, *Adv. Fiber Mater.* **2020**, 2, 123.
- [28] Y. Liu, F. Wu, Y. Ding, B. Zhu, Y. Su, X. Zhu, *Adv. Fiber Mater.* **2019**, 1, 152.
- [29] C. Cheng, S. Li, A. Thomas, N. A. Kotov, R. Haag, *Chem. Rev.* **2017**, 117, 1826.
- [30] Z. Zhang, L. H. Klausen, M. Chen, M. Dong, *Small* **2018**, 14, 1801983.
- [31] Y. Xia, S. Li, C. Nie, J. Zhang, S. Zhou, H. Yang, M. Li, W. Li, C. Cheng, R. Haag, *Appl. Mater. Today* **2019**, 16, 518.
- [32] C. X. Nie, L. Ma, S. Li, X. Fan, Y. Yang, C. Cheng, W. F. Zhao, C. S. Zhao, *Nano Today* **2019**, 26, 57.
- [33] L. Ma, M. Zhou, C. He, S. Li, X. Fan, C. Nie, H. Luo, L. Qiu, C. Cheng, *Green Chem.* **2019**, 21, 4887.
- [34] Y. Xia, X. Fan, H. Yang, L. Li, C. He, C. Cheng, R. Haag, *Small* **2020**, 16, 2003010.
- [35] L. Ma, F. Jiang, X. Fan, L. Wang, C. He, M. Zhou, S. Li, H. Luo, C. Cheng, L. Qiu, *Adv. Mater.* **2020**, 32, 2003065.
- [36] C. J. Wan, L. Q. Zhu, Y. H. Liu, P. Feng, Z. P. Liu, H. L. Cao, P. Xiao, Y. Shi, Q. Wan, *Adv. Mater.* **2016**, 28, 3557.

- [37] C. Cheng, J. Zhang, S. Li, Y. Xia, C. Nie, Z. Shi, J. L. Cuellar-Camacho, N. Ma, R. Haag, *Adv. Mater.* **2018**, *30*, 1705452.
- [38] C. Cheng, S. Li, Y. Xia, L. Ma, C. Nie, C. Roth, A. Thomas, R. Haag, *Adv. Mater.* **2018**, *30*, 1802669.
- [39] F. Paulus, D. Steinhilber, P. Welker, D. Mangoldt, K. Licha, H. Depner, S. Sigrist, R. Haag, *Polym. Chem.* **2014**, *5*, 5020.
- [40] Q. Ran, X. Xu, P. Dey, S. Yu, Y. Lu, J. Dzubiella, R. Haag, M. Ballauff, *J. Chem. Phys.* **2018**, *149*, 163324.
- [41] Z. Zhu, Y. Liu, Y. Xue, X. Cheng, W. Zhao, J. Wang, R. He, Q. Wan, X. Pei, *ACS Appl. Mater. Interfaces* **2019**, *11*, 36141.
- [42] C. Fasting, C. A. Schalley, M. Weber, O. Seitz, S. Hecht, B. Koksich, J. Dervede, C. Graf, E.-W. Knapp, R. Haag, *Angew. Chem., Int. Ed.* **2012**, *51*, 10472.
- [43] Y. Xia, C. Cheng, R. Wang, H. Qin, Y. Zhang, L. Ma, H. Tan, Z. Gu, C. Zhao, *Polym. Chem.* **2014**, *5*, 5906.
- [44] J. Vonnemann, S. Liese, C. Kuehne, K. Ludwig, J. Dervede, C. Böttcher, R. R. Netz, R. Haag, *J. Am. Chem. Soc.* **2015**, *137*, 2572.
- [45] M. F. Gholami, D. Lauster, K. Ludwig, J. Storm, B. Ziem, N. Severin, C. Böttcher, J. P. Rabe, A. Herrmann, M. Adeli, R. Haag, *Adv. Funct. Mater.* **2017**, *27*, 1606477.
- [46] S. Dupont, L. Morsut, M. Aragona, E. Enzo, S. Giullitti, M. Cordenonsi, F. Zanconato, J. L. Digabel, M. Forcato, S. Bicchato, N. Elvassore, S. Piccolo, *Nature* **2011**, *474*, 179.
- [47] W. Deng, F. Shao, Q. He, Q. Wang, W. Shi, Q. Yu, X. Cao, C. Feng, S. Bi, J. Chen, P. Ma, Y. Li, A. Gong, S. Tong, J. Yu, M. Spector, X. Xu, Z. Zhang, *Adv. Mater.* **2019**, *31*, 1806861.
- [48] B. Zhao, X. Wei, W. Li, R. S. Udan, Q. Yang, J. Kim, J. Xie, T. Ikenoue, J. Yu, L. Li, P. Zheng, K. Ye, A. Chinnaiyan, G. Halder, Z.-C. Lai, K.-L. Guan, *Genes Dev.* **2007**, *21*, 2747.
- [49] C. M. Madl, B. L. LeSavage, R. E. Dewi, K. J. Lampe, S. C. Heilshorn, *Adv. Sci.* **2019**, *6*, 1801716.
- [50] I. Lian, J. Kim, H. Okazawa, J. Zhao, B. Zhao, J. Yu, A. Chinnaiyan, M. A. Israel, L. S. B. Goldstein, R. Abujarour, S. Ding, K.-L. Guan, *Genes Dev.* **2010**, *24*, 1106.
- [51] Y. Li, H. Feng, H. Gu, D. W. Lewis, Y. Yuan, L. Zhang, H. Yu, P. Zhang, H. Cheng, W. Miao, W. Yuan, S.-Y. Cheng, S. M. Gollin, T. Cheng, *Nat. Commun.* **2013**, *4*, 2174.
- [52] H. Zheng, W.-M. Yu, J. Shen, S. Kang, D. Hambardzumyan, J. Y. Li, Y. Shen, A. M. Kenney, J. Chen, C.-K. Qu, *Sci. Adv.* **2018**, *4*, eaat2681.
- [53] J. Chen, S. Boyle, M. Zhao, W. Su, K. Takahashi, L. Davis, M. DeCaestecker, T. Takahashi, M. D. Breyer, C.-M. Hao, *J. Am. Soc. Nephrol.* **2006**, *17*, 1283.
- [54] A. A. Sosunov, E. Guilfoyle, X. Wu, G. M. McKhann, J. E. Goldman, *J. Neurosci.* **2013**, *33*, 7439.
- [55] J. Lu, X. Zhong, H. Liu, L. Hao, C. T.-L. Huang, M. A. Sherafat, J. Jones, M. Ayala, L. Li, S.-C. Zhang, *Nat. Biotechnol.* **2016**, *34*, 89.
- [56] P. A. Nistor, P. W. May, F. Tamagnini, A. D. Randall, M. A. Caldwell, *Biomaterials* **2015**, *61*, 139.
- [57] G. Kouroupi, E. Taoufik, I. S. Vlachos, K. Tsioras, N. Antoniou, F. Papastefanaki, D. Chroni-Tzartou, W. Wrasidlo, D. Bohl, D. Stellas, P. K. Politis, K. Vekrellis, D. Papadimitriou, L. Stefanis, P. Bregestovski, A. G. Hatzigeorgiou, E. Masliah, R. Matsas, *Proc. Natl. Acad. Sci. U. S. A.* **2017**, *114*, E3679.
- [58] B. Ji, H. Kaneko, T. Minamimoto, H. Inoue, H. Takeuchi, K. Kumata, M.-R. Zhang, I. Aoki, C. Seki, M. Ono, M. Tokunaga, S. Tsukamoto, K. Tanabe, R.-M. Shin, T. Minamihisamatsu, S. Kito, B. J. Richmond, T. Suhara, M. Higuchi, *J. Neurosci.* **2016**, *36*, 11544.
- [59] K. W. Dunn, M. M. Kamocka, J. H. McDonald, *Am. J. Physiol. Cell Physiol.* **2011**, *300*, C723.